Available online at www.sciencedirect.com
ScienceDirect
Journal of Sound and Vibration 324 (2009) 297–316
JOURNAL OF SOUND AND VIBRATION
www.elsevier.com/locate/jsvi

A continuous piecewise internal friction model of hysteresis for use in dynamical simulations

Christos Spitas*

Department of Production Engineering and Management, Technical University of Crete, 58 Filolaou Street, GR 11633, Greece

Received 13 November 2008; received in revised form 27 January 2009; accepted 2 February 2009
Handling Editor: M.P. Cartmell
Available online 17 March 2009

Abstract

The suitability of the internal friction models by Reid [Free vibration and hysteretic damping, *Journal of the Royal Aeronautical Society* 69 (1956) 283] and Muravskii [On frequency independent damping, *Journal of Sound and Vibration* 274 (2004) 653–668] for modelling hysteretic damping is investigated. Time-domain dynamical simulations of Reid's model reveal the presence of artefacts, which cause significant errors and solution stiffness in sub-resonant conditions. Muravskii's non-analytical modification of Reid's model is shown to be inconsistent with its primary goal of achieving continuity at the points of strain-rate reversal. An analytical constitutive equation for this model is derived and its implications discussed; the model is shown to be equivalent to Reid's model. Attempting to embody the original concept of Muravskii, a new variant of Reid's model is proposed, replacing the discontinuous sign function found in Reid and Muravskii with a continuous piecewise function. The new model is tested and compared to its predecessors for various steady state and transient oscillatory conditions, including resonance, and is found to be a competent alternative to the robust, but very frequency-sensitive, viscous model.

1. Introduction

Hysteresis, otherwise referred to as frequency-independent damping, is a phenomenon that has proven difficult to model efficiently in the time domain. The convenient viscous damping model is a poor choice of modelling hysteresis, due to its strong frequency dependence; however it is often the tool of choice, because of its continuity and very simple form. The complex stiffness formulation is well known to be limited to steady-state frequency-domain solutions only, giving non-causal responses when ported to the time domain [1]. Alternatives with far superior accuracy have only found acceptance in those situations where high accuracy is paramount and the overall systems are rather simple, i.e. of these alternatives the Bouc–Wen model [2] is likely to be the most capable, but it is very complicated, introducing an extra non-physical variable and a strongly nonlinear differential equation, whereas the characterisation of its four parameters requires complicated procedures. It is therefore hard to recommend such heavyweight models for the average simulation and

*Tel.: +30 6973038267.
E-mail addresses: cspitas@geartech.net, cspitas@yahoo.com (C. Spitas).

0022-460X/$ - see front matter © 2009 Elsevier Ltd. All rights reserved.
doi:10.1016/j.jsv.2009.02.006

Nomenclature

A	surface area	m	mass
E	Young's modulus	t	time
f	frequency	x	displacement
F	force	$\widehat{x}$	displacement amplitude
H	hysteresis function	ε	strain
k	spring stiffness	$\widehat{\varepsilon}$	strain amplitude
l	length	η	hysteresis coefficient
		σ	stress
		ω	cyclic frequency

certainly their modelling and computation overheads make their use in systems with many degrees of freedom a challenge.

Among the more lightweight alternatives, the nonlinear model by Reid [3] is based on a rather literal interpretation of the term 'internal friction' that was used originally for hysteresis [4] and was elaborated by Theodorsen [5]. The model attributes the elastic energy dissipation to a Coulomb friction mechanism and gives predictions for the energy loss per cycle proportional to the square amplitude and independent of the strain rate, or oscillation frequency; these closely match real hysteresis. The constitutive equation of the model has an attractive simplicity and has been studied, among others, by Caughey [1], Beucke [6], and lately Muravskii [7]. The model does have obvious drawbacks, however, in that its through-zero hysteretic loops in strain–stress space look quite artificial, but mostly in that it is fundamentally discontinuous at the points of strain-rate reversal.

Muravskii [7] attempted a modification of Reid's model, in order to remedy the noted discontinuity. The modified model essentially consists of a 'Reid spring' in series with a perfectly elastic spring. No analytical constitutive equation was offered for this model, but instead a piecewise description of its function. While Muravskii produced some results in support of this model, the present work conducts a fresh investigation to verify the consistency between the defining spring structure and Muravskii's piecewise functional description. This is done by developing an analytical constitutive equation for the spring structure and analysing it.

In the next step, the present work embarks on a new variation of Reid's model. The fundamental reason for the discontinuity at the point of strain-rate reversal is identified and a continuous piecewise function is used to provide the necessary transition from positive to negative strain rate in a continuous manner. The resulting model is tested and compared with the Reid model for various steady state and transient oscillatory conditions, including resonance.

2. Macro- and micro-modelling and non-dimensional modelling

Hysteresis is understood to be a fundamental property of material micro-structure. If this hysteretic behaviour is observable in a macro-structure, it should therefore be considered as the resultant of the infinitesimal phenomena contributing to it, integrated over a volume of material. In any case, it is generally scientifically more robust, and therefore recommended, to integrate micro-models to obtain macro-models, than to assume the validity of macro-models in the micro-cosmos, even if this seems intuitively obvious.

Nonetheless, many researchers have used springs to visualise physical models of hysteresis and have, as a result, used terms such as spring stiffness, displacement, velocity and force to describe it. It is implied that these macro-models have been conceived to apply at the micro-structural level as well. However, in line with the recommendation given above, this work will adopt a micro-structural viewpoint where possible, thereby referring to elementary volumes of material under plane strain uniaxial tension/compression, rather than springs. From this viewpoint models are described in terms of Young's modulus, strain, strain rate, stress, etc. The presented theory is certainly and directly extensible to the macro-cosmos (where its main utility eventually lies) and the reader is cautioned to observe the equivalence shown in Fig. 1.

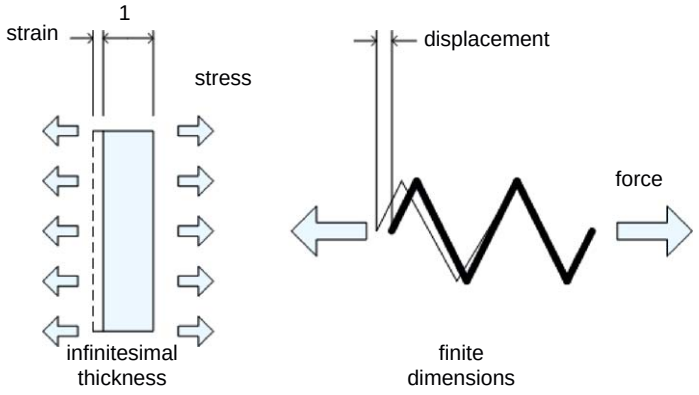

Fig. 1. Equivalence between a micro-model and a macro-model for hysteretic behaviour.

A unification of the micro- and macro-models can be achieved using non-dimensionalisation. Strain is already non-dimensional, and a non-dimensional stress can be obtained thus:

$$\varepsilon' = \varepsilon \tag{1}$$

$$\sigma' = \frac{\sigma}{E} \tag{2}$$

For structures, the strain equivalent for small deflections x of a spring with length l will be

$$x' = \frac{x}{l} \tag{3}$$

while a stress equivalent for a spring stiffness k is

$$F' = \frac{F}{kl} \tag{4}$$

Under the common non-dimensional formulation, the elastic equilibrium of a linear elastic material or structure can be described simply as

$$\sigma' = \varepsilon' \quad \text{or} \quad F' = x' \tag{5}$$

whereas any state involving hysteresis may be thought to satisfy the following relationship:

$$\sigma' = H\varepsilon' \quad \text{or} \quad F' = Hx' \tag{6}$$

We shall call H the hysteresis function and it will be seen that this formulation is applicable to the models in Sections 3 and 5. This should not be taken to mean that Eq. (6) is universally applicable to all, or even most, hysteretic models: Its only purpose is to facilitate comparison of the particular models examined in this paper.

Henceforth, throughout this work the possibility to switch between dimensional descriptions will be exploited freely to best serve the particular needs of each section (i.e. the discussion of Muravskii's model and the dynamical simulations best lend themselves to a macroscopical approach), and the general non-dimensional description of Eqs. (1)–(6) should be borne in mind.

3. Reid's model

This nonlinear model for hysteresis was first introduced by Reid [3]. It models hysteresis after friction, and is expressed as:

$$\sigma = E\left(\varepsilon + \eta|\varepsilon|\frac{\dot{\varepsilon}}{|\dot{\varepsilon}|}\right) \tag{7}$$

Let us consider a continuous mapping from $\mathbb{R}^+$ to $\mathbb{R}^2$, such that each strain–stress state can be described as $(\varepsilon(t), \sigma(t))$, where $t \geqslant 0$ and $\varepsilon(t)$ is continuous, and a periodic behaviour of amplitude $\widehat{\varepsilon}$, such that $\varepsilon(t) = \varepsilon(t + 2\pi/\omega)$, $\sigma(t) = \sigma(t + 2\pi/\omega)$.

The non-dimensional strain–stress hysteresis loop, i.e. for $\eta = 0.1$, is plotted in Fig. 2 and the elastic energy dissipated per cycle is calculated from

$$w_h = \int_{2\pi/\omega} \sigma \, \mathrm{d}\varepsilon \tag{8}$$

Noticing that Eq. (7) is of a piecewise nature, equivalently written as

$$\sigma = \begin{cases} E(\varepsilon + \eta|\varepsilon|), & \dot{\varepsilon} \geqslant 0 \\ E(\varepsilon - \eta|\varepsilon|), & \dot{\varepsilon} < 0 \end{cases}$$

and taking advantage of the hysteresis loop symmetry, we obtain from Eqs. (7) and (8):

$$w_h = 2\left[\int_0^{\widehat{\varepsilon}} E(1+\eta)\varepsilon \, \mathrm{d}\varepsilon + \int_{\widehat{\varepsilon}}^0 E(1-\eta)\varepsilon \, \mathrm{d}\varepsilon\right]$$

$$w_h = 2E\eta\left(\int_0^{\widehat{\varepsilon}} \varepsilon \, \mathrm{d}\varepsilon + \int_0^{\widehat{\varepsilon}} \varepsilon \, \mathrm{d}\varepsilon\right)$$

Hence

$$w_h = 2E\eta\widehat{\varepsilon}^2 \tag{9}$$

Clearly, this work is proportional to $\widehat{\varepsilon}^2$ and completely independent of the strain rate, hence also of the cyclic frequency, if the cyclical loading is taken to be periodic.

The discontinuity at the points of strain-rate reversal is calculated:

$$\Delta\sigma = \left|\lim_{t \to t_o^+} \sigma - \lim_{t \to t_o^-} \sigma\right| = 2E\eta\,\widehat{\varepsilon} \neq 0 \quad \text{for every } t_o > 0 \text{ such that } \dot{\varepsilon} = 0 \tag{10}$$

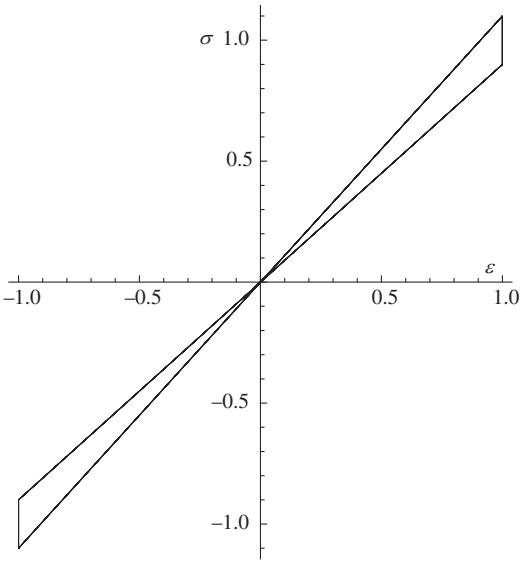

Fig. 2. Hysteresis loop in non-dimensional strain–stress space, as predicted by Reid and calculated from Eq. (7).

where the condition $\dot{\varepsilon} = 0$ signifies strain-rate reversal. This discontinuity will be shown in subsequent simulations to introduce artificial excitations at double the oscillation frequency. The produced artefacts are expected to become increasingly significant near resonance, limiting the usefulness of Reid's model.

From Eqs. (1), (2), (6) and (7), the non-dimensional hysteresis function corresponding to Reid's model, with all its noted shortcomings (through-zero loop, discontinuity), is deduced:

$$H = 1 + \eta \frac{|\varepsilon'|}{\varepsilon'} \frac{\dot{\varepsilon}'}{|\dot{\varepsilon}'|}$$

$$H = 1 + \eta \,\mathrm{sign}(\varepsilon')\mathrm{sign}(\dot{\varepsilon}') \tag{11}$$

4. Muravskii's modified model

This model has been proposed by Muravskii [7] as an extension of Reid's model explicitly aiming to 'eliminate discontinuities in the force, which are inherent in the hysteretic model'. The model comprises a 'Reid spring' in series with a perfectly elastic spring, as shown in Fig. 3, and Muravskii offers the following description with reference to the displacement–force plane, avoiding to give a constitutive equation:

'If a point (x, F) lies at a moment on the line with angle coefficient k_α or k_β and the velocity changes its sign passing the zero value, then the point begins to move along the line with angle coefficient k_0, and the value F remains continuous. For time intervals in which the velocity does not change its sign, there are linear relations between Δx and ΔF with coefficients k_α, k_β or k_0. This description, following from the behaviour of the mechanical system shown in Fig. 4, is sufficient for obtaining a relation between the force and displacement, and can serve instead of a constitutive equation.'

The corresponding coefficient definitions are given as

$$k_\alpha = \frac{1}{\dfrac{1}{k_0} + \dfrac{1}{k_1(1+\eta_1)}}, \quad k_\beta = \frac{1}{\dfrac{1}{k_0} + \dfrac{1}{k_1(1-\eta_1)}} \tag{12}$$

In addition to the loop shown in Fig. 4, Muravskii gives the following prediction for the elastic energy dissipated per cycle:

$$w_h = 2k\eta\hat{x}^2 \frac{\beta - 1 - \eta}{\beta - 1 + \eta} \tag{13}$$

where

$$k = \frac{k_\alpha + k_\beta}{2}, \quad \beta = \frac{2k_0}{k_\alpha + k_\beta}, \quad \eta = \frac{k_\alpha - k_\beta}{k_\alpha + k_\beta}$$

It will be shown hereafter that the described behaviour is inconsistent with the spring model definition in Fig. 3. An exact analytical constitutive equation for this model can be found as follows. The equilibrium

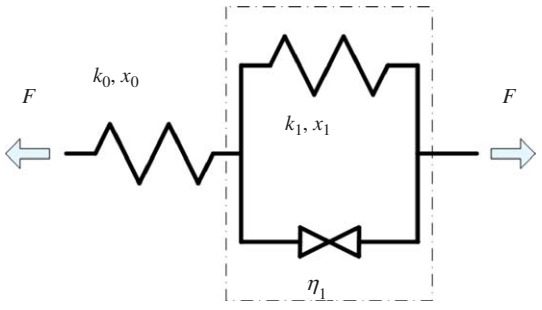

Fig. 3. Muravskii's definition of a continuous hysteresis model.

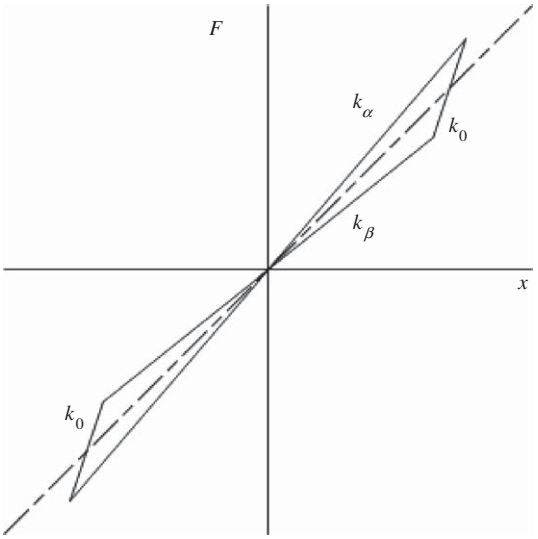

Fig. 4. Muravskii's prediction of the displacement–force plot (from Ref. [7]).

equations are

$$F = k_0 x_0 \tag{14}$$

$$F = k_1\left(x_1 + \eta_1 |x_1| \frac{\dot{x}_1}{|\dot{x}_1|}\right) \tag{15}$$

Eq. (15) can be re-written in a form more useful for further manipulation:

$$F = k_1 x_1\left(1 + \eta_1 \frac{|x_1|}{x_1}\frac{\dot{x}_1}{|\dot{x}_1|}\right) \tag{16}$$

It is easy to observe that all 'springs' of the model are in phase, therefore considering x to be the total deflection of the combined spring ($x = x_1 + x_2$, see Fig. 3):

$$\frac{|x_1|}{x_1} = \frac{|x|}{x} \quad \text{and} \quad \frac{\dot{x}_1}{|\dot{x}_1|} = \frac{\dot{x}}{|\dot{x}|} \tag{17}$$

Substituting Eq. (17) into Eq. (16) yields

$$F = k_1 x_1\left(1 + \eta_1 \frac{|x|}{x}\frac{\dot{x}}{|\dot{x}|}\right) \tag{18}$$

Compatibility of the deflections requires that

$$x = x_0 + x_1 \tag{19}$$

Substituting Eqs. (14) and (18) into Eq. (19) yields

$$x = \frac{F}{k_0} + \frac{F}{k_1\left(1 + \eta_1 \dfrac{|x|}{x}\dfrac{\dot{x}}{|\dot{x}|}\right)} \tag{20}$$

The analytical formulation for the modified internal friction model is obtained from Eq. (20) after some manipulation:

$$F = \frac{1}{\dfrac{1}{k_0} + \dfrac{1}{k_1\left(1 + \eta_1 \dfrac{|x|}{x}\dfrac{\dot{x}}{|\dot{x}|}\right)}} x \tag{21}$$

As is the case with all other hysteresis models, Eq. (21) is generally applicable to strain–stress states as well as to displacement–force states, accommodating all model scales. As expected, Eq. (21) converges to Eq. (7), the original Reid model, as $k_0 \to \infty$.

Considering an arbitrary cyclical loading of amplitude $\hat{x} = 1$ and assuming $k_0 = 10$, $k_1 = 1.0$, $\eta_1 = 0.1$, the displacement–force plot can be calculated from Eq. (21) and is plotted in Fig. 5. Different choices of parameters and amplitude yield essentially the same form. This result is distinctly different from Muravskii's description, shown in Fig. 4. Quite notably, an unforeseen and yet persistent discontinuity similar to Reid's can be seen at the points of strain-rate reversal (Fig. 5).

Taking advantage of the hysteresis loop symmetry, the work per cycle can be calculated from Eqs. (8) and (21), adapted for notation:

$$w_h = 2\left(\int_0^{\hat{x}} \frac{1}{\dfrac{1}{k_0} + \dfrac{1}{k_1(1+\eta_1)}} x\,\mathrm{d}x + \int_{\hat{x}}^{0} \frac{1}{\dfrac{1}{k_0} + \dfrac{1}{k_1(1-\eta_1)}} x\,\mathrm{d}x\right)$$

$$w_h = 2\left(\int_0^{\hat{x}} k_\alpha x\,\mathrm{d}x - \int_0^{\hat{x}} k_\beta x\,\mathrm{d}x\right)$$

$$w_h = (k_\alpha - k_\beta)\hat{x}^2 \tag{22}$$

Eq. (22) can be seen to be quite similar to Eq. (9) of Reid's model (by choosing $k_\alpha - k_\beta = 2E\eta$). It is, however, notably different from Eq. (13), or its equivalent form:

$$w_h = (k_\alpha - k_\beta)\hat{x}^2 \frac{\beta - 1 - \eta}{\beta - 1 + \eta}$$

where obviously $k_\alpha \neq k_\beta$ and therefore $\eta = (k_\alpha - k_\beta)/(k_\alpha + k_\beta) \neq 0$ and $(\beta - 1 - \eta)/(\beta - 1 + \eta) \neq 1$.

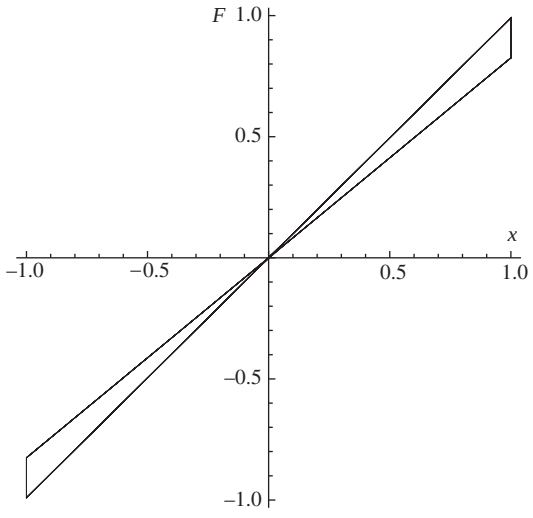

Fig. 5. Hysteresis loop in displacement–force space calculated from Eq. (21).

The dissipated elastic energy is proportional to $\hat{x}^2$ and completely independent of the strain rate, hence also of the frequency, if the cyclical loading is taken to be periodic.

The discontinuity at the points of strain-rate reversal is calculated:

$$\Delta\sigma = \left| \lim_{t \to t_o^+} \sigma - \lim_{t \to t_o^-} \sigma \right| = (k_\alpha - k_\beta)\hat{x} \neq 0 \quad \text{for every } t_o > 0 \text{ such that } \dot{x} = 0 \tag{23}$$

where the condition $\dot{\varepsilon} = 0$ signifies strain-rate reversal. At this point, there can be no doubt that the models by Reid and Muravskii are equivalent. Both exhibit the same discontinuity at the points of strain-rate reversal, have the same overall loop shape and give the same prediction for the dissipated elastic energy. Muravskii's model employs three parameters, but the effective number of parameters is two, namely k_α and k_β.

It should be noted that Muravskii's *functional description* of his model, plotted in Fig. 4, is consistent with the continuous behaviour that he sought, even if it has been proven to be inconsistent with the spring model of Fig. 3. However an analytical constitutive equation cannot be derived from that description in an obvious way.

5. Continuous piecewise model

As can be concluded from the above analysis, the question of extending Reid's model to eliminate discontinuities is still open. By studying Eq. (7) and Fig. 2, the following remarks are made:

(a) The discontinuities are entirely caused by the sign function $\dot{\varepsilon}/|\dot{\varepsilon}|$.
(b) Any composite model produced by combining 'Reid springs' and/or perfectly elastic springs, as was done by Muravskii, will still manifest the discontinuities of its components. Therefore, no such combination can exist that will achieve a continuous response.
(c) In light of the above, it is proposed that the sign function in Reid's model be replaced with a continuous piecewise function that will achieve a similar result.

Generally, this function, which will be denoted hereafter as $h(\dot{\varepsilon})$, should satisfy the following conditions:

$$h = \begin{cases} 1, & \dot{\varepsilon} \geqslant \dot{\varepsilon}_i \\ -1, & \dot{\varepsilon} \leqslant -\dot{\varepsilon}_i \end{cases}, \quad h \text{ is continuous for every } |\dot{\varepsilon}| < \dot{\varepsilon}_1 \tag{24}$$

where $\dot{\varepsilon}_i > 0$ is an appropriately chosen strain-rate value delimiting a 'transition regime', which will be henceforth called 'transition strain rate'. The hysteretic model itself is formulated as follows:

$$\sigma = E\left[1 + \eta h(\dot{\varepsilon})\frac{|\varepsilon|}{\varepsilon}\right]\varepsilon \tag{25}$$

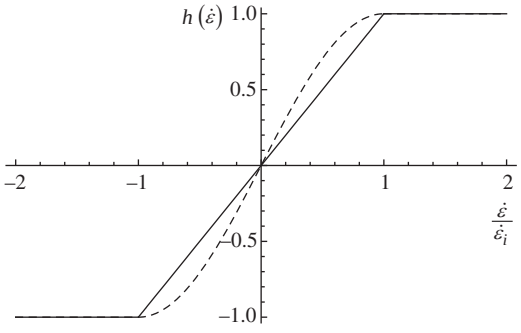

Fig. 6. Non-dimensional plot of continuous piecewise replacements for the sign function as per Eq. (27) (solid line) and Eq. (28) (dashed line).

From Eqs. (1), (2), (6) and (25) the non-dimensional hysteresis function is deduced:

$$H = 1 + \eta h(\dot{\varepsilon}')\frac{|\varepsilon'|}{\varepsilon'}$$

$$H = 1 + \eta h(\dot{\varepsilon}')\text{sign}(\varepsilon') \tag{26}$$

We are therefore looking for continuous functions conformant to Eq. (24) to replace the sign function of Reid. Aiming for the simplest form possible, two attractive embodiments for $h(\dot{\varepsilon})$ are (see Fig. 6)

$$h = \begin{cases} 1, & \dot{\varepsilon} \geqslant \dot{\varepsilon}_i \\ \dfrac{\dot{\varepsilon}}{\dot{\varepsilon}_i}, & |\dot{\varepsilon}| < \dot{\varepsilon}_i,\ \dot{\varepsilon}_i > 0 \\ -1, & \dot{\varepsilon} \leqslant -\dot{\varepsilon}_i \end{cases} \tag{27}$$

or

$$h = \begin{cases} 1, & \dot{\varepsilon} \geqslant \dot{\varepsilon}_i \\ \sin\left(\pi\dfrac{\dot{\varepsilon}}{2\dot{\varepsilon}_i}\right) & |\dot{\varepsilon}| < \dot{\varepsilon}_i,\ \dot{\varepsilon}_i > 0 \\ -1, & \dot{\varepsilon} \leqslant -\dot{\varepsilon}_i \end{cases} \tag{28}$$

The function of Eq. (28) has a continuous first derivative as well. It is easy to understand that the hysteresis loops resulting from any of the embodiments of Eq. (25) are dependent, to an extent, on the strain rate. It is recognised that infinite other possible embodiments exist that satisfy the basic requirement of Eq. (24), but exploring them is beyond the scope of this paper and, as will be seen in the subsequent analysis, unnecessary.

If a harmonic oscillation of the strain is forced:

$$\varepsilon = \widehat{\varepsilon}\ \sin\ \omega t \tag{29}$$

the elastic energy dissipated per cycle is calculated as follows, assuming that $h(\dot{\varepsilon})$ is given by Eq. (27). First let us insert Eq. (29) into (25):

$$\sigma = E\left[1 + \eta h(\widehat{\varepsilon}\,\omega\ \cos\ \omega t)\frac{|\widehat{\varepsilon}\ \sin\ \omega t|}{\widehat{\varepsilon}\ \sin\ \omega t}\right]\widehat{\varepsilon}\ \sin\ \omega t$$

$$\sigma = E\left[1 + \eta h(\widehat{\varepsilon}\,\omega\ \cos\ \omega t)\frac{|\sin\ \omega t|}{\sin\ \omega t}\right]\widehat{\varepsilon}\ \sin\ \omega t \tag{30}$$

Considering that $-\pi/\omega \leqslant t < \pi/\omega$ (noting that $2\pi/\omega$ equals one period), we observe that

$$\frac{|\sin\ \omega t|}{\sin\ \omega t} = -1, \quad -\frac{\pi}{\omega} \leqslant t < 0$$

and

$$\frac{|\sin\ \omega t|}{\sin\ \omega t} = 1, \quad 0 \leqslant t < \frac{\pi}{\omega} \tag{31}$$

The salient points in Eq. (27) occur when

$$|\dot{\varepsilon}| = \dot{\varepsilon}_i$$

$$\widehat{\varepsilon}\,\omega\ \cos\ \omega t = \pm\dot{\varepsilon}_i$$

$$t = \pm\frac{1}{\omega}\cos^{-1}\pm\frac{\dot{\varepsilon}_i}{\widehat{\varepsilon}\,\omega} \tag{32}$$

Therefore Eq. (27) becomes

$$h=\begin{cases} 1, & -\dfrac{1}{\omega}\cos^{-1}\dfrac{\dot{\varepsilon}_i}{\widehat{\varepsilon}\,\omega}<t<\dfrac{1}{\omega}\cos^{-1}\dfrac{\dot{\varepsilon}_i}{\widehat{\varepsilon}\,\omega} \\ \dfrac{\widehat{\varepsilon}\,\omega\cos\omega t}{\dot{\varepsilon}_i}, & \begin{cases} -\dfrac{1}{\omega}\cos^{-1}-\dfrac{\dot{\varepsilon}_i}{\widehat{\varepsilon}\,\omega}\leqslant t\leqslant -\dfrac{1}{\omega}\cos^{-1}\dfrac{\dot{\varepsilon}_i}{\widehat{\varepsilon}\,\omega} \\ \dfrac{1}{\omega}\cos^{-1}\dfrac{\dot{\varepsilon}_i}{\widehat{\varepsilon}\,\omega}\leqslant t\leqslant\dfrac{1}{\omega}\cos^{-1}-\dfrac{\dot{\varepsilon}_i}{\widehat{\varepsilon}\,\omega} \end{cases}, \ \dot{\varepsilon}_i>0 \\ -1, & \begin{cases} -\dfrac{\pi}{\omega}\leqslant t<-\dfrac{1}{\omega}\cos^{-1}-\dfrac{\dot{\varepsilon}_i}{\widehat{\varepsilon}\,\omega} \\ \dfrac{1}{\omega}\cos^{-1}-\dfrac{\dot{\varepsilon}_i}{\widehat{\varepsilon}\,\omega}<t\leqslant\dfrac{\pi}{\omega} \end{cases} \end{cases} \tag{33}$$

The results of Eqs. (33) and (31) are plotted in Fig. 7 vs. non-dimensional time assuming $\dot{\varepsilon}_i/\widehat{\varepsilon}\,\omega=0.3$ (as no particular material or system is considered in this paper, the choice of this value is arbitrary and is provided purely for reproducibility of the presented results). Their combined product is plotted in Fig. 8 and compared to the corresponding term from Reid's model. The inclined continuous segments occur at the transition strain rate intervals.

The non-dimensional stress response is calculated from Eqs. (25) to (27) and plotted in Fig. 9, next to the prediction by Reid's model, calculated from Eq. (7).

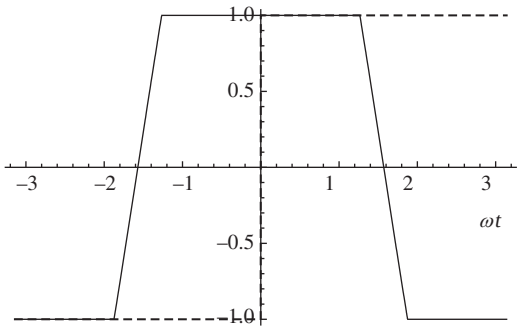

Fig. 7. Plot of Eq. (33) (solid line) and Eq. (31) (dashed line) in non-dimensional time ωt assuming $\dot{\varepsilon}_i/\widehat{\varepsilon}\,\omega=0.3$.

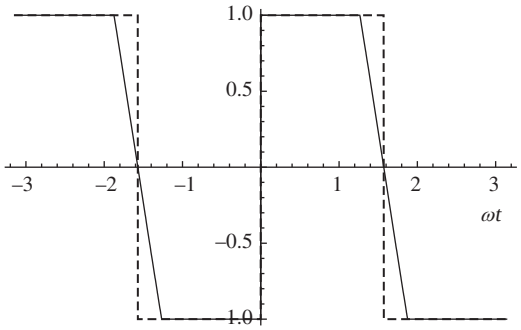

Fig. 8. Plot of $h(\dot{\varepsilon})(|\varepsilon|/\varepsilon)$ (continuous piecewise model, Eq. (27), solid line) and $(\dot{\varepsilon}/|\dot{\varepsilon}|)(|\varepsilon|/\varepsilon)$ (Reid's model, dashed line) in non-dimensional time ωt assuming $\dot{\varepsilon}_i/\widehat{\varepsilon}\,\omega=0.3$.

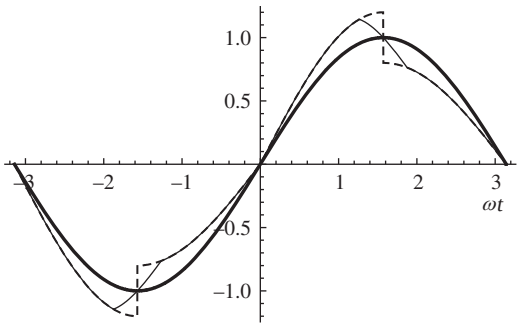

Fig. 9. Non-dimensional plots of: (a) harmonic strain excitation (thick line), (b) stress prediction of continuous piecewise model as per Eqs. (25)–(27) (thin line), and (c) stress prediction of original Reid's model (Eq. (7), dashed line) in non-dimensional time ωt assuming $\dot{\varepsilon}_i/\widehat{\varepsilon}\,\omega = 0.3$.

The elastic energy dissipated per cycle is

$$w_h = \int_{2\pi/\omega} \sigma \, \mathrm{d}\varepsilon$$

Taking advantage of the hysteresis loop symmetry, this integral can be broken down to its piecewise components as per Eqs. (31) and (33):

$$\begin{aligned}\frac{1}{2}w_h = &\int_{t=0}^{(1/\omega)\cos^{-1}(\dot{\varepsilon}_i/\widehat{\varepsilon}\,\omega)} E(1+\eta)\widehat{\varepsilon}^2 \sin\omega t \, \mathrm{d}(\sin\omega t) \\ &+ \int_{t=(1/\omega)\cos^{-1}(\dot{\varepsilon}_i/\widehat{\varepsilon}\,\omega)}^{(1/\omega)\cos^{-1}-(\dot{\varepsilon}_i/\widehat{\varepsilon}\,\omega)} E\left[1+\eta\frac{\widehat{\varepsilon}\,\omega\cos\omega t}{\dot{\varepsilon}_i}\right]\widehat{\varepsilon}^2 \sin\omega t \, \mathrm{d}(\sin\omega t) \\ &+ \int_{t=(1/\omega)\cos^{-1}-(\dot{\varepsilon}_i/\widehat{\varepsilon}\,\omega)}^{\pi/\omega} E(1-\eta)\widehat{\varepsilon}^2 \sin\omega t \, \mathrm{d}(\sin\omega t), \quad \frac{\dot{\varepsilon}_i}{\widehat{\varepsilon}\,\omega} \leqslant 1 \end{aligned} \tag{34}$$

The indefinite integrals in Eq. (34) are solved as follows:

$$\int E(1\pm\eta)\widehat{\varepsilon}^2 \sin\omega t \, \mathrm{d}(\sin\omega t) = -\tfrac{1}{2}E\widehat{\varepsilon}^2(1\pm\eta)\cos^2\omega t \tag{35}$$

$$\int E\left[1\pm\eta\frac{\widehat{\varepsilon}\,\omega\cos\omega t}{\dot{\varepsilon}_i}\right]\widehat{\varepsilon}^2 \sin\omega t \, \mathrm{d}(\sin\omega t) = -\frac{1}{4}E\widehat{\varepsilon}^2\left[\cos 2\omega t + \eta\frac{\widehat{\varepsilon}\,\omega\cos\omega t}{\dot{\varepsilon}_i}(\cos\omega t \mp \cos 3\omega t)\right] \tag{36}$$

By substituting Eqs. (35) and (36) into Eq. (34) and calculating for the respective integration intervals, we obtain

$$\begin{aligned}\frac{1}{2}w_h = &-\frac{1}{2}E\widehat{\varepsilon}^2\left[\left(\frac{\dot{\varepsilon}_i}{\widehat{\varepsilon}\,\omega}\right)^2 - 1\right](1+\eta) \\ &+\frac{2}{3}E\widehat{\varepsilon}^2\left(\frac{\dot{\varepsilon}_i}{\widehat{\varepsilon}\,\omega}\right)^2\eta \\ &-\frac{1}{2}E\widehat{\varepsilon}^2\left[\left(\frac{\dot{\varepsilon}_i}{\widehat{\varepsilon}\,\omega}\right)^2 - 1\right](-1+\eta)\end{aligned}$$

which can be further simplified to

$$w_h = 2E\eta\widehat{\varepsilon}^2\left[1-\frac{1}{3}\left(\frac{\dot{\varepsilon}_i}{\widehat{\varepsilon}\,\omega}\right)^2\right], \quad \frac{\dot{\varepsilon}_i}{\widehat{\varepsilon}\,\omega}\leqslant 1 \tag{37}$$

Any choice of the parameter $\dot{\varepsilon}_i$ outside the conditional bounds set in Eqs. (34) and (37) will lead to a different calculation of the dissipated elastic energy:

$$w_h = 2\int_{t=0}^{\pi/\omega} E\left[1+\eta\frac{\widehat{\varepsilon}\,\omega\cos\,\omega t}{\dot{\varepsilon}_i}\right]\widehat{\varepsilon}^2\sin\,\omega t\,\mathrm{d}(\sin\,\omega t), \quad \frac{\dot{\varepsilon}_i}{\widehat{\varepsilon}\,\omega}>1 \tag{38}$$

which, after manipulations similar as before, resolves to

$$w_h = 2E\eta\widehat{\varepsilon}^2\frac{2}{3}\left(\frac{\dot{\varepsilon}_i}{\widehat{\varepsilon}\,\omega}\right)^{-1}, \quad \frac{\dot{\varepsilon}_i}{\widehat{\varepsilon}\,\omega}>1 \tag{39}$$

Eqs. (37) and (39) can be unified as follows:

$$w_h = 2E\eta\widehat{\varepsilon}^2\delta \tag{40}$$

where

$$\delta=\begin{cases}1-\frac{1}{3}\left(\frac{\dot{\varepsilon}_i}{\widehat{\varepsilon}\,\omega}\right)^2, & \frac{\dot{\varepsilon}_i}{\widehat{\varepsilon}\,\omega}\leqslant 1\\ \frac{2}{3}\left(\frac{\dot{\varepsilon}_i}{\widehat{\varepsilon}\,\omega}\right)^{-1}, & \frac{\dot{\varepsilon}_i}{\widehat{\varepsilon}\,\omega}>1\end{cases} \tag{41}$$

Eq. (40), which gives the dissipated elastic energy per cycle for the continuous piecewise model, can be directly compared to Eq. (9) for Reid's model. They differ by the factor δ, the implications of which are investigated as follows.

In a harmonic oscillation, as in Eq. (29), the strain rate is clearly bounded as follows:

$$|\dot{\varepsilon}|\leqslant\widehat{\varepsilon}\,\omega \tag{42}$$

As a first thought, if we can anticipate the amplitude and frequency conditions for a studied physical system and therefore the upper bound for $\widehat{\varepsilon}\,\omega$, it makes sense to subject the choice of the parameter $\dot{\varepsilon}_i$ to the same bounds, obtaining from Eq. (40):

$$\tfrac{2}{3}\leqslant\delta\leqslant 1 \tag{43}$$

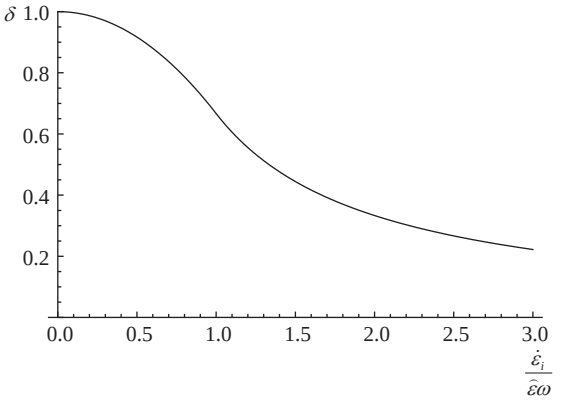

Fig. 10. Factor δ vs. $\dot{\varepsilon}_i/\widehat{\varepsilon}\,\omega$.

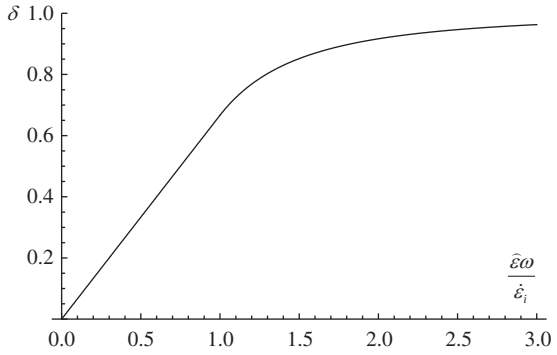

Fig. 11. Factor δ vs. $\hat{\varepsilon}\,\omega/\dot{\varepsilon}_i$.

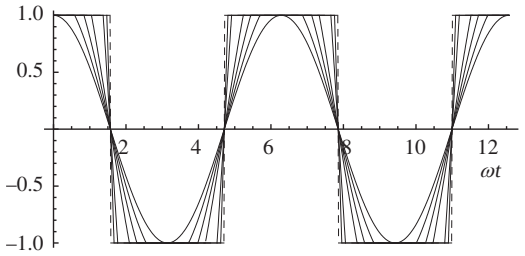

Fig. 12. Effect of increasing the amplitude $\hat{\varepsilon}$ and/or frequency ω of harmonic oscillations on the function $h(\dot{\varepsilon})$ vs. non-dimensional time ωt. The dotted line corresponds to the bounding condition $\hat{\varepsilon}\,\omega \to \infty$ and is identical to the sign function of Reid's model.

Any choice of the parameter $\dot{\varepsilon}_i$ outside the bounds of Eq. (39) will lead to

$$0 \leqslant \delta < \tfrac{2}{3} \tag{44}$$

A plot of the factor δ as a function of $\dot{\varepsilon}_i/\hat{\varepsilon}\,\omega$ is given in Fig. 10.

Evidently, the choice of $\dot{\varepsilon}_i$ can influence the predictions of the model for given oscillatory conditions (amplitude and frequency). Because $\dot{\varepsilon}_i$ is typically chosen before these conditions are known, it is more insightful to plot the factor δ vs. $\hat{\varepsilon}\,\omega/\dot{\varepsilon}_i$, as in Fig. 11. In this plot it can be readily seen that in the amplitude–frequency range $\hat{\varepsilon}\,\omega/\dot{\varepsilon}_i > 2$, where $0.917 < \delta \leqslant 1$, the model exhibits a fairly reliable behaviour, with an error in predicted energy dissipation of well under 10 percent. It is therefore sufficient to select a low enough $\dot{\varepsilon}_i$ in advance. If the model should encounter unexpectedly low amplitude–frequency conditions, then the error can rise appreciably, but gradually. In any case, the results can be post-processed to reveal such conditions and repeated with a more suitable choice for $\dot{\varepsilon}_i$.

Further on parameter sensitivity, the effect of increasing the amplitude $\hat{\varepsilon}$ and/or the frequency ω of harmonic oscillations on the function $h(\dot{\varepsilon})$ is plotted in Fig. 12 vs. non-dimensional time ωt. It can be seen that, as $\hat{\varepsilon}\,\omega \to \infty$, a bounding condition (envelope) is reached, where $h(\dot{\varepsilon})$ converges to the sign function of Reid's model. Conversely, under very low amplitude and/or frequency conditions the transitional segments become predominant, until the constant value segments of $h(\dot{\varepsilon})$ vanish completely. This situation corresponds to the leftmost side of Fig. 11, where $\hat{\varepsilon}\,\omega/\dot{\varepsilon}_i < 1$, and is associated with rapidly increasing errors. The effect of increasing amplitude and frequency on the hysteresis loop in strain–stress space can be seen in Figs. 13a and b.

It has been well established in the above discussion that, as $\dot{\varepsilon}_i \to 0$, the continuous piecewise model converges to Reid's original model. Therefore, it can be seen that an optimal choice exists between the higher values for $\dot{\varepsilon}_i$, which increase error and amplitude–frequency sensitivity, and the lower values for $\dot{\varepsilon}_i$, which produce sharper strain-rate reversal transitions and related artefacts. It does not make sense to give a universal recommendation, as any choice will have to consider the detailed context of any simulation. Some rough guidelines are given in Table 1, based on the discussion so far and the results of several test simulations (including the dynamical simulations discussed later) under varying parameters.

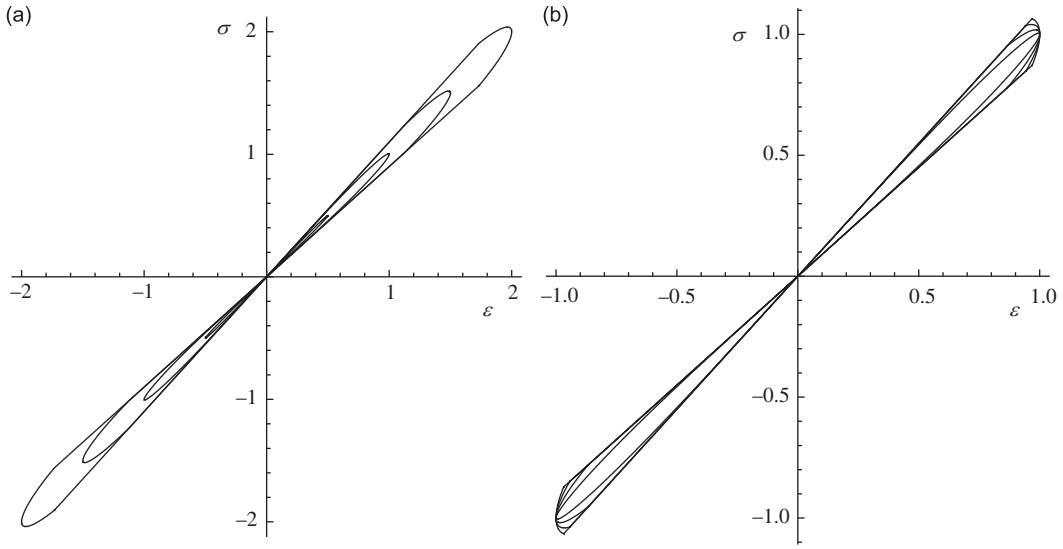

Fig. 13. (a) Plot of hysteresis loops of increasing amplitude in non-dimensional strain–stress space at constant frequency and (b) plot of hysteresis loops of increasing frequency in non-dimensional strain–stress space at constant amplitude.

Table 1
Rough guidelines for parameter selection of the continuous piecewise hysteresis model.

Expected conditions	Recommendation for choosing $\dot{\varepsilon}_i$
Wide-ranging amplitudes and/or frequencies, possibly near resonance	$\dot{\varepsilon}_i \approx 0.5 \min\{\widehat{\varepsilon}\,\omega\}$
Narrow-ranging amplitudes and/or frequencies, especially in low frequency range	$\dot{\varepsilon}_i \approx \min\{\widehat{\varepsilon}\,\omega\}$

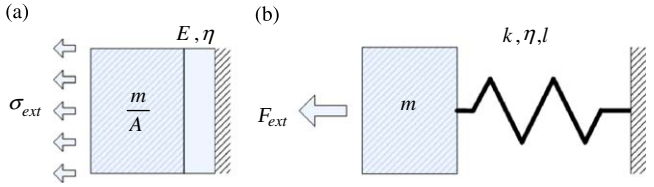

Fig. 14. (a) Micro-embodiment of a general mass–hysteretic elastic system and (b) macro-embodiment of a general mass–hysteretic elastic system.

Eq. (28) has also been used with the continuous piecewise model; it has been found to produce nearly identical results as Eq. (27). It can therefore be concluded that the exact shape of the function $h(\dot{\varepsilon})$, or the continuity of its first derivatives, are not nearly as important to model behaviour as is the selection of the parameter $\dot{\varepsilon}_i$.

The characterisation of the model parameters E and η can be done exactly as for Reid's model, while compensating for the estimated error of δ due to the selection of $\dot{\varepsilon}_i$, based on Eq. (41) and the guidelines given.

To understand the method of correction, consider a Reid model with parameters E_o, η_o and dissipated elastic energy $w_{h,o}$ calculated at an amplitude $\widehat{\varepsilon}_o$ and frequency ω_o. If we select $\dot{\varepsilon}_i \neq 0$ (i.e. $\dot{\varepsilon}_i = 0.5\widehat{\varepsilon}_o\omega_o$), then at the calibration conditions the continuous piecewise model will yield, by using Eqs. (40) and (41), an energy estimate:

$$w_h = w_{h,o}\delta_o \quad (\text{i.e. } \delta_o = 0.917) \tag{45}$$

Therefore the model parameters should be corrected as follows:

$$E = E_o \tag{46}$$

$$\eta = \frac{1}{\delta_o}\eta_o \tag{47}$$

6. Dynamical simulations

Simulations have been conducted in the time domain for the basic single degree-of-freedom system. Figs. 14a and b illustrate the micro- and macro-embodiments of a general mass–hysteretic elastic system. The dynamic equation for the macroscopic system in Fig. 14b is well known:

$$m\ddot{x} + kHx = F_{ext} \tag{48}$$

where H may be replaced by the appropriate expressions for Reid's model, presented in Eq. (11), and its continuous piecewise extension, presented in Eq. (26).

Eq. (41) can be made non-dimensional by dividing it by ml:

$$\frac{\ddot{x}}{l} + \frac{k}{m}H\frac{x}{l} = \frac{F_{ext}}{ml}$$

$$+\frac{k}{m}H \quad = \frac{F_{ext}}{ml} \tag{49}$$

The system cyclic eigenfrequency is

$$\omega_n = \sqrt{\frac{k}{m}} \tag{50}$$

The elastic energy dissipated per cycle due to hysteresis was assumed:

$$w_h = 0.04k\hat{x}^2 \tag{51}$$

An equivalent viscous system with the same energy dissipation rate per cycle has also been studied for comparison. Its dynamic equation is

$$\ddot{x}' + \frac{c}{m}\dot{x}' + \frac{k}{m}\ x' = \frac{F_{ext}}{ml} \tag{52}$$

The energy dissipated per cycle for the viscous equivalent at a given oscillation frequency is

$$w_h = \pi kc\hat{x}^2\omega^2 \tag{53}$$

Therefore from Eqs. (51) and (53) the viscous damping coefficient may be calibrated for different oscillation frequencies as follows:

$$c = \frac{0.04}{\pi\omega^2} \tag{54}$$

Steady-state simulations were conducted assuming harmonic external excitation of varying frequency spanning the $0.1\omega_n - 3.0\omega_n$ range. Figs. 15a–17a show the state response vs. non-dimensional time $\omega_n t$ for three interesting excitation frequencies: $0.2\omega_n$ (low frequency), $0.5\omega_n$, and $1.0\omega_n$ (resonance). The corresponding power spectra vs. non-dimensional frequency $2\pi f/\omega_n$ (increments of the natural frequency) were computed numerically over steady-state non-dimensional time intervals of $300\omega_n$ without any window processing and are plotted in Figs. 15b–17b. The solution of the dynamic equations was conducted in the Mathematica™ environment using, for the most part, default settings. The Reid and continuous piecewise models were simulated numerically.

Based on these results, several observations have been made:

(1) Reid's model becomes stiff and runs into convergence problems for frequencies under $0.45\omega_n - 0.5\omega_n$. The reason can be identified in the acceleration plot in Fig. 15a, where very high frequency components

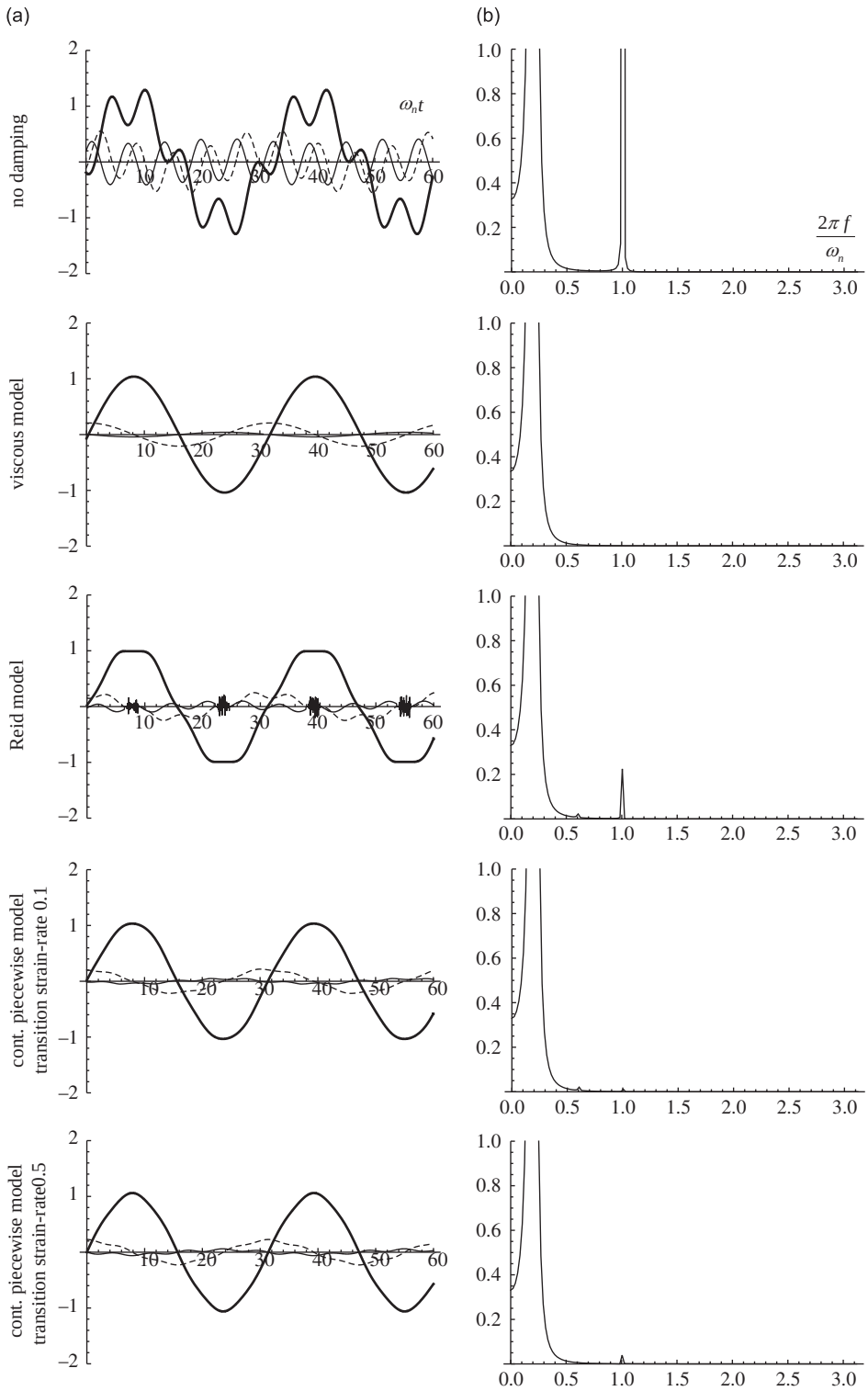

Fig. 15. (a) Non-dimensional response to a harmonic excitation at $0.2\omega_n$ vs. non-dimensional time $\omega_n t$ (strain: thick line, strain rate: dashed line, acceleration: thin line) and (b) non-dimensional power spectrum of the response to a harmonic excitation at $0.2\omega_n$ vs. non-dimensional frequency $2\pi f/\omega_n$.

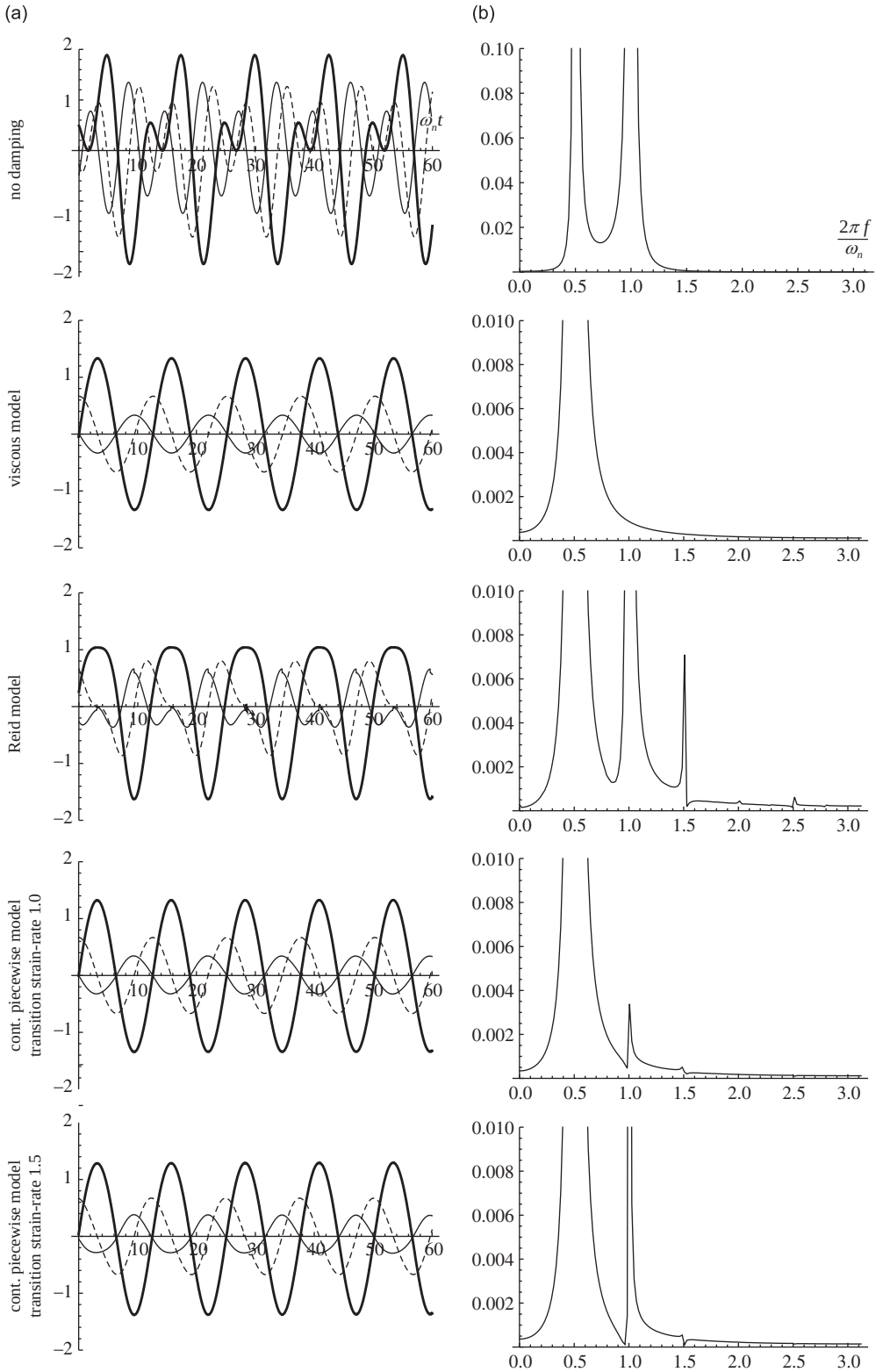

Fig. 16. (a) Non-dimensional response to a harmonic excitation at $0.5\omega_n$ vs. non-dimensional time $\omega_n t$ (strain: thick line, strain rate: dashed line, acceleration: thin line) and (b) non-dimensional power spectrum of the response to a harmonic excitation at $0.5\omega_n$ vs. non-dimensional frequency $2\pi f/\omega_n$.

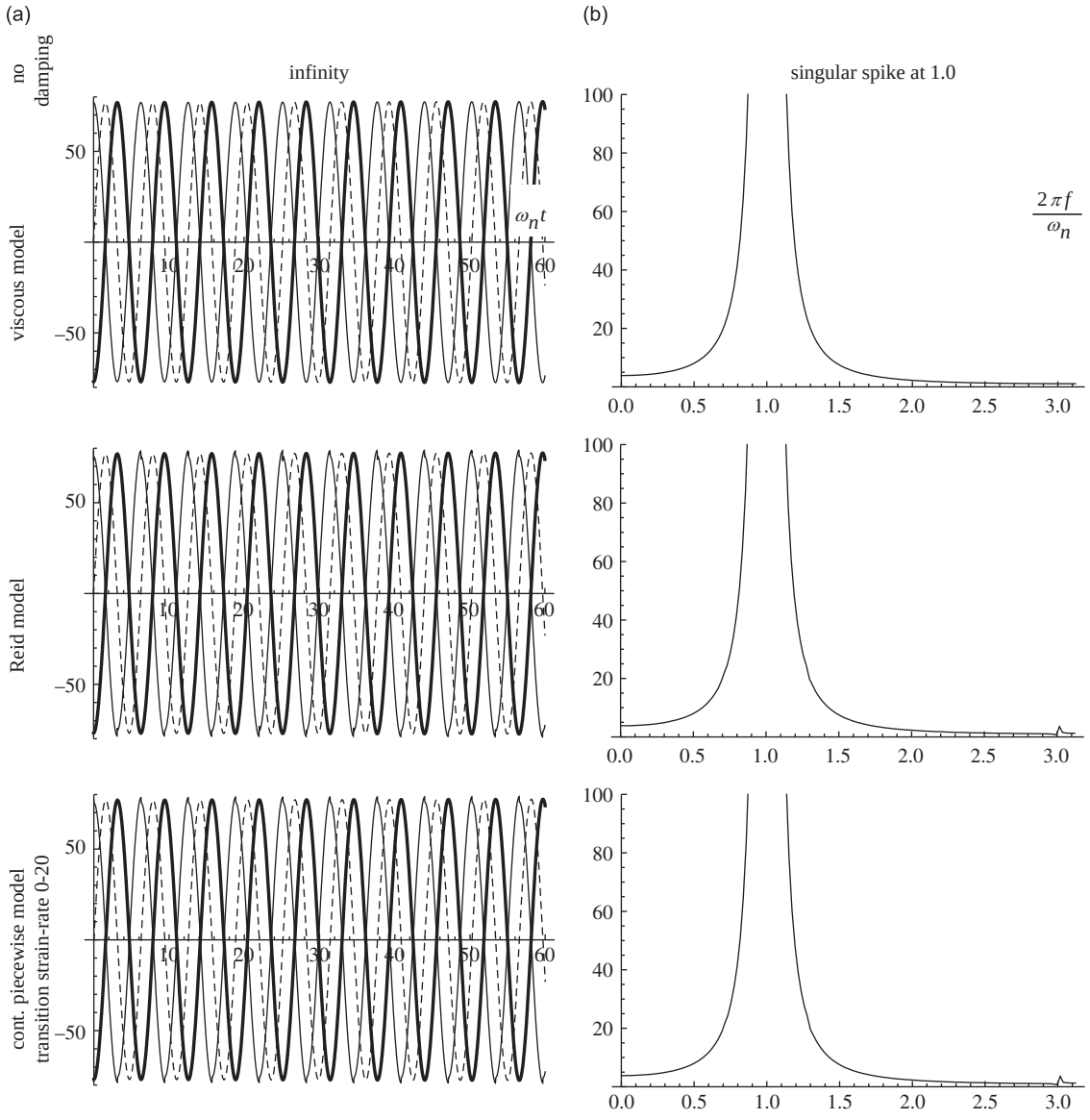

Fig. 17. (a) Non-dimensional response to a harmonic excitation at ω_n (resonance) vs. non-dimensional time $\omega_n t$ (strain: thick line, strain rate: dashed line, acceleration: thin line) and (b) non-dimensional power spectrum of the response to a harmonic excitation at ω_n (resonance) vs. non-dimensional frequency $2\pi f/\omega_n$.

are observed around the points of zero strain rate. This can be directly traced back to the discontinuity of Eq. (4), which produces a strong artificial excitation.

(2) At sub-critical frequencies, the waveform produced by Reid's model looks quite artificial when compared to all other models. Discontinuities in the acceleration plot are clearly evident even at $0.5\omega_n$, as can be seen in Figs. 15a and 16a

(3) Reid's model produces a frequency artefact at the natural frequency for all sub-critical frequencies, as can be seen in Figs. 15b–16b. At $0.5\omega_n$ important artefacts appear also at higher harmonics, as can be seen in Fig. 16b, likely due to the fact that the natural frequency is a multiple of the oscillation frequency. All artefacts have been found to vanish as frequency increases to resonance, as can be seen in Fig. 17b, and this is also true beyond the resonant frequency.

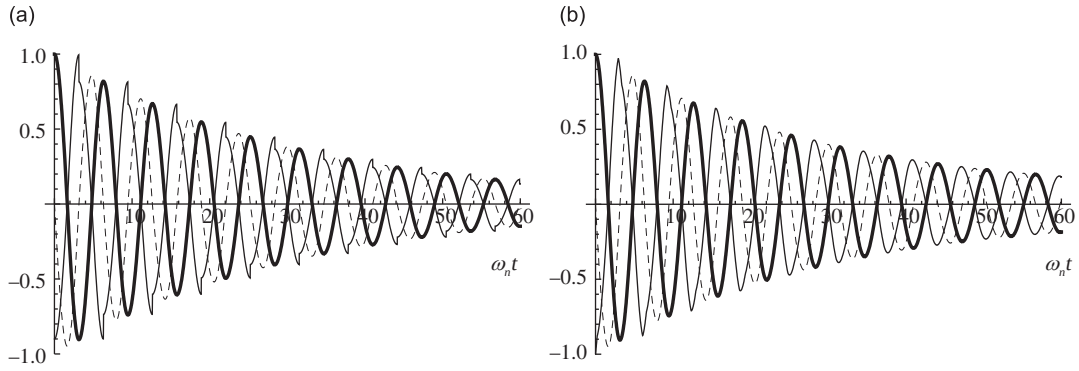

Fig. 18. Free vibration after an initial excitation vs. non-dimensional time $\omega_n t$ using Reid's model (left) and the continuous piecewise model (right) with $\dot{x}_i = 0.2$ (displacement: thick line, velocity: dashed line, acceleration: thin line). A high value $w_h = 0.2k\bar{x}^2$ was used in order to better illustrate the differences.

(4) The same artefacts can be seen, albeit at a reduced scale, in the continuous piecewise model. Their magnitude is seen to depend strongly on the choice of the transition strain rate. Fig. 16b reveals that this effect is not monotonous, and increasing the non-dimensional transition rate $\dot{x}'_i/\bar{x}'\omega$ beyond 1.0 at $0.5\omega_n$ causes a strengthening of the primary artefact, to levels almost comparable to the Reid model.
(5) The waveforms of the continuous piecewise model are themselves, in spite of point 4, quite 'natural' in appearance, mostly comparable to the waveforms of the viscous model, and at no time does the solution of the dynamic equation become stiff. The choice of the transition strain rate does not seem critical in this respect.
(6) The resonant response of all simulated models is practically identical. As all models were specifically calibrated to yield the same elastic energy dissipation per cycle at the excitation frequency, it can be concluded that the choice of model for the study of resonant conditions is not critical. Reid's model does, however, still present minor artefacts in the time domain, as can be seen after careful inspection of the acceleration plot in Fig. 17a.
(7) The Reid and continuous piecewise models do not require re-calibration to adapt to different frequencies, as is the case with the viscous model.

The free vibration transient response of the Reid and the continuous piecewise model was also simulated, assuming an off-equilibrium initial strain condition. The results are plotted in Fig. 18 vs. non-dimensional time $\omega_n t$. Unusually high damping was used, in order to better illustrate the differences. For most purposes the responses can be considered equivalent; however the artificial jumps in acceleration predicted by the Reid model, the cause for which can be traced back to Eq. (10), adversely affect convergence speed and, of course, the accuracy of the acceleration prediction itself.

7. Conclusion

Although Muravskii's non-analytical extension of Reid's hysteresis model has been proven inconsistent, the internal friction damping concept for hysteresis has been refined successfully by substituting Reid's sign function with a continuous piecewise function, to induce smooth acceleration at the points of strain-rate reversal. Analytical treatment of the new model has been combined with dynamical simulations at various oscillation frequencies to develop guidelines for calibrating the parameters. The simulation results show that the model suppresses many of the artefacts associated with strain-rate reversal and results in reasonably accurate waveforms, comparable to those obtained by properly calibrated viscous damping. This and the fact that it inherits its predecessor's basic insensitivity to changing frequency make it a competent alternative to the widely used, but very frequency-sensitive, viscous model.

References

[1] T.K. Caughey, A. Vijayaraghavan, Free and forced oscillations of a dynamic system with "linear hysteretic damping" (non-linear theory), *International Journal of Non-Linear Mechanics* 5 (1970) 533–555.
[2] Y.-K. Wen, Method for random vibration of hysteretic systems, *Journal of Engineering Mechanics* 102 (1976) 249–263.
[3] T.J. Reid, Free vibration and hysteretic damping, *Journal of the Royal Aeronautical Society* 69 (1965) 283.
[4] A.L. Kimball, D.F. Lovell, Internal friction in solids, *Physics Review* 30 (1927) 948.
[5] T. Theodorsen, I.E. Garrick, Mechanism of flutter, a theoretical and experimental investigation of the flutter problem, NACA Report no. 685, 1940.
[6] K.E. Beucke, J.M. Kelly, Equivalent linearizations for practical hysteretic systems, *International Journal of Non-Linear Mechanics* 23 (1985) 211–238.
[7] G.B. Muravskii, On frequency independent damping, *Journal of Sound and Vibration* 274 (2004) 653–668.